—Original—

Estimation of Microvascular Dysfunction by Using ^{13}N-Ammonia Positron Emission Tomography with Quantitative Myocardial Blood Flow Analysis in Chronic Coronary Syndrome

Shogo Imai[1], Tomonari Kiriyama[1], Koji Kanaya[2], Satoe Aoyama[2], Hitoshi Takano[3] and Shin-ichiro Kumita[1]

[1]Department of Radiology, Nippon Medical School, Tokyo, Japan
[2]Clinical Imaging Center for Healthcare, Nippon Medical School, Tokyo, Japan
[3]Department of Cardiovascular Medicine, Nippon Medical School, Tokyo, Japan

Background: Although coronary artery disease (CAD) is characterized by epicardial atherosclerosis and microvascular disease, the importance of evaluating microvascular dysfunction has not been sufficiently recognized in clinical practice. We estimated microvascular disease severity by assessing hyperemic microvascular resistance (MVR), as determined by absolute quantification of myocardial blood flow (MBF) with ^{13}N-ammonia positron emission tomography-myocardial perfusion imaging (PET-MPI).

Methods: We retrospectively collected data for 23 CAD patients who underwent both stress/rest PET-MPI and invasive coronary angiography (CAG) with fractional flow reserve (FFR) measurement. Among 30 vessels for which FFR measurement was performed, 13 had a low FFR (FFR ≤0.75). For each patient, myocardial segments of a standard 17-segment model were assigned to the stenotic myocardial area perfused by the FFR-measured vessel and a reference normal-perfusion area based on PET-MPI and the coronary distribution on CAG. Hyperemic MVR was calculated by using the formula, hyperemic MVR = hyperemic mean blood pressure × FFR/hyperemic MBF of the stenotic vessel.

Results: A strong negative correlation was observed between hyperemic MVR and hyperemic MBF in the reference normal-perfusion area ($R = -0.758$, $P<0.001$).

Conclusion: Microvascular disease severity in chronic CAD can be estimated by hyperemic MBF of the normal-perfusion area with ^{13}N-ammonia PET-MPI. (J Nippon Med Sch 2023; 90: 228–236)

Key words: coronary artery disease, coronary microvascular dysfunction, positron emission tomography, myocardial blood flow, myocardial perfusion image

Introduction

Coronary artery disease (CAD) comprises 2 main elements: epicardial atherosclerosis with flow-limiting stenosis and coronary microvascular dysfunction (CMD). Although epicardial stenosis has been considered the main target of percutaneous coronary intervention (PCI) and coronary artery bypass grafting in patients with CAD, multiple recent studies have reported that CMD is related to cardiovascular outcomes and have focused on the importance of coronary microcirculation[1–5]. Several studies have suggested invasive or noninvasive techniques for indirect evaluation of microvascular function, but these techniques are not common in clinical practice[6,7].

Coronary flow reserve (CFR) acquired from myocardial perfusion positron emission tomography (PET) reflects the degree of epicardial stenosis and CMD[3]. CFR in a myocardial area without significant epicardial stenosis is regulated by microvascular function[6]. In contrast, hyperemic myocardial blood flow (MBF) varies among healthy persons without epicardial stenosis[8], and the normal range and clinical value of hyperemic MBF have not

Correspondence to Shogo Imai, MD, Department of Radiology, Nippon Medical School, 1–1–5 Sendagi, Bunkyo-ku, Tokyo 113–8602, Japan
E-mail: shogoimai@nms.ac.jp
https://doi.org/10.1272/jnms.JNMS.2023_90-213
Journal Website (https://www.nms.ac.jp/sh/jnms/)

Table 1 Patient characteristics

Variable	n = 23
Male	15 (65%)
Age (years)	74.3 ± 8.1
Body mass index (kg/m^2)	23.3 ± 3.9
Hypertension	20 (87%)
Diabetes mellitus	6 (26%)
Dyslipidemia	21 (91%)
Smoking	14 (61%)
Obesity*	6 (26%)
Previous PCI	10 (43%)
Coronary stenosis	
1VD	10 (43%)
2VD	11 (48%)
3VD	2 (9%)

Data are presented as mean ± SD or number (%).
*Obesity was defined as a BMI greater than or equal to 25.
PCI, percutaneous coronary intervention; 1VD, one-vessel disease; 2VD, two-vessel disease; 3VD, three-vessel disease

been determined. Moreover, although the COURAGE (Clinical Outcomes Utilizing Revascularization and Aggressive Drug Evaluation) and ISCHEMIA (International Study of Comparative Health Effectiveness with Medical and Invasive Approaches) trials found that invasive reperfusion therapy for a stenotic lesion with myocardial ischemia did not reduce the incidence of cardiac events, the pandemic of heart failure has arrived worldwide concern[9,10]. Because CMD is considered a primary reason for heart failure with preserved ejection fraction (HFpEF) and ischemia with no obstructive coronary artery (INOCA), evaluation of CMD is gaining importance in routine clinical practice. Therefore, there is a need for a simple, noninvasive method to evaluate CMD.

We hypothesize that variation in hyperemic MBF in normal areas is mostly defined by differences in vasodilatory capacity, and that the vasodilatory capacity of coronary arterioles similarly deteriorates in myocardial areas, with and without significant stenosis, because of aging and disease. To develop a noninvasive method to determine CMD severity, this study examined the association between vasodilator capacity and hyperemic MBF or CFR by using quantitative perfusion data derived from ^{13}N-ammonia PET and invasively measured fractional flow reserve (FFR).

Materials and Methods

Study Population

Data were retrospectively collected from the medical records of patients with suspected or known CAD who underwent ^{13}N-ammonia myocardial perfusion PET (PET-MPI) between November 1, 2012, and December 31, 2017. Among these patients, data from 23 patients (15 males; mean age 74.3 ± 8.1 years) with at least 1 stenosis (1-vessel disease, 10 patients; 2-vessel disease, 11 patients; 3-vessel disease, 2 patients), as determined by invasive coronary angiography with FFR measurement within 6 months before or after ^{13}N-ammonia PET-MPI, were analyzed. Patients with a history of coronary bypass surgery, heart transplantation, or moderate or severe valvular disease were excluded. In addition, patients with severe atrioventricular block, sick sinus syndrome, long QT syndrome, severe hypotension, and bronchial asthma were excluded because they could not be loaded with adenosine. The baseline characteristics of the patients are summarized in **Table 1**. Among the 23 patients with chronic CAD, 6 had typical chest pain, 7 had atypical chest pain, and 10 were asymptomatic. In addition, 20 had arterial hypertension, 6 had diabetes mellitus, 21 had dyslipidemia, and 14 were present or past smokers. Previous coronary angioplasty was performed in 10 patients. Written informed consent was obtained from all included patients. This study was approved by the relevant ethics committee (Ethics Committee of Nippon Medical School Clinical Imaging Center for Healthcare, reference number: K-02) and performed in accordance with the ethical standards of the Declaration of Helsinki.

Image Acquisition

PET scanning was performed with a GEMINI TF-16 (Philips Medical Systems) hybrid time-of-flight PET/CT scanner, and PET acquisition was performed in the three-dimensional list mode. Scatter correction was performed with a time-of-flight single-scatter simulation algorithm, while attenuation correction was based on CT scans. All participants were carefully instructed to refrain from caffeine intake for 24 h before the PET study. Each participant was injected with 370 MBq (10 mCi) of ^{13}N-ammonia into the right antecubital vein, irrespective of body weight, followed by a 30-mL saline flush at rest. After a 40-50-min interval, the same doses were injected during pharmacological stress with less than 5 min of continuous intravenous infusion of adenosine (120-144 μg/kg/min), which started 3 min before ammonia injection. Dynamic imaging was initiated just before injection and extended for 10 min. Heart rate, blood pressure, and

a 12-lead electrocardiogram were recorded every minute during and after adenosine infusion, along with continuous electrocardiogram monitoring. Twenty-three dynamic frames were reconstructed (20 × 6 s, 2 × 30 s, and 1 × 60 s). For visual analysis, short-axis, horizontal long-axis, and vertical long-axis images were reconstructed with frames between 4 and 10 min. The reconstruction parameters for time-of-flight ordered subset expectation maximization were set at 3 iterations, and 33 subsets were optimized for clinical application.

Quantification of Absolute MBF

Quantitative analyses of absolute MBF (mL/min/g) were performed using the PMOD software package (version 3.4, PMOD Technologies Ltd., Zurich, Switzerland). Regions of interest were semi-automatically placed on the myocardium and the biventricular blood pool in each slice. Myocardial and blood-pool time-activity curves, generated from the dynamic frames, were fitted with the tracer kinetic model. We adopted the DeGrado 1-compartment model, which assumes that there is no metabolic trapping[11]. Data for the first 4 min (24 frames) were used for curve fitting. The estimated stress MBF was expressed in coronary territories and myocardial segments by using a standard 17-segment model of the American Heart Association (**Fig. 1B**). The CFR was calculated as the ratio of hyperemic MBF to rest MBF in each myocardial segment.

Invasive Coronary Angiography and FFR Measurement

Invasive coronary angiography was performed to assess epicardial stenosis and evaluate the severity of the stenosis by measuring the FFR. Before the estimation of stenosis, intracoronary nitroglycerin was administered to enlarge coronary diameters. Stenosis was evaluated from at least 2 orthogonal directions with quantitative coronary angiography, and significant stenosis was defined as >50% diameter stenosis. To induce maximal coronary hyperemia, adenosine or intracoronary papaverine was administered intravenously for estimation of FFR, which was calculated as the ratio of mean distal intracoronary pressure to mean arterial pressure. Evaluation of the severity of stenosis and assessment of FFR signals were performed by experienced interventional cardiologists.

Image Analysis

Two of the authors (S.I. and T.K.), nuclear medicine specialists with 5 and 13 years of experience, respectively, identified stenotic coronary myocardial segments perfused by the stenotic vessel for which FFR had been measured by referring to static PET images and coronary angiography (CAG). The 17 myocardial segments were assigned to the coronary arteries on the basis of individual coronary distribution. The averaged hyperemic MBF of the stenotic myocardial segments was regarded as the MBF in stenotic coronary territory ($MBF_{stenotic}$). **Figure 1** shows a CAD patient with mid left ascending coronary artery stenosis, which decreased the FFR by 0.78. In this case, the area perfused by the mid left ascending coronary artery consisted of myocardial segments #7, 8, 13, 14, 15, and 17 (red area in **Fig. 1C**). Myocardial segments #2 and #3 (gray diagonal stripes in **Fig. 1C**), which represent the basal interventricular septum, were excluded in the estimation because of low counts in the membranous septum. Myocardial segments with apparently erroneous MBF (a hyperemic MBF of ≥4.0 and a difference of ≥0.5 between adjacent segments with no visual difference) were also excluded from the analysis. Myocardial segments #3 and #9 (yellow area in **Fig. 1C**) were excluded because of erroneous values for this patient. The average hyperemic MBF of the myocardial segments with the 3 highest MBF values was used as the normal reference hyperemic MBF (MBF_{remote}). In **Figure 1**, the normal-perfusion area was defined as myocardial segments #5, 11, and 16 (blue area in **Fig. 1C**).

Microvascular resistance (mm Hg・min・g/mL) in the hyperemic state was calculated by using a previously published equation[12]: Hyperemic microvascular resistance = (hyperemic mean blood pressure ・ FFR)/hyperemic MBF (**Fig. 1D**). Microvascular resistance (MVR) was expressed as the value obtained by dividing the distal coronary pressure (P_d) by absolute MBF. P_d was considered identical to the value obtained by multiplying FFR by the brachial blood pressure measured during an adenosine stress PET scan, because FFR is the ratio of P_d to aortic pressure (P_a) during maximal hyperemia and P_a is assumed to be equal to peripheral mean blood pressure measured in the limbs.

Hyperemic MVR in stenotic and remote areas was calculated with the above equation, and the results were labeled $_{Est.}MVR_{stenotic}$ and $_{Est.}MVR_{remote}$, respectively. In calculating $_{Est.}MVR_{remote}$, the FFR was assumed to be 1. Thus, the equations to calculate each of them were:

$_{Est.}MVR_{stenotic}$ = (hyperemic mean blood pressure ・ FFR)/hyperemic $MBF_{stenotic}$

$_{Est.}MVR_{remote}$ = hyperemic mean blood pressure/hyperemic MBF_{remote}.

Statistical Analysis

Categorical variables are expressed as numbers and relative frequencies (percentages), and continuous vari-

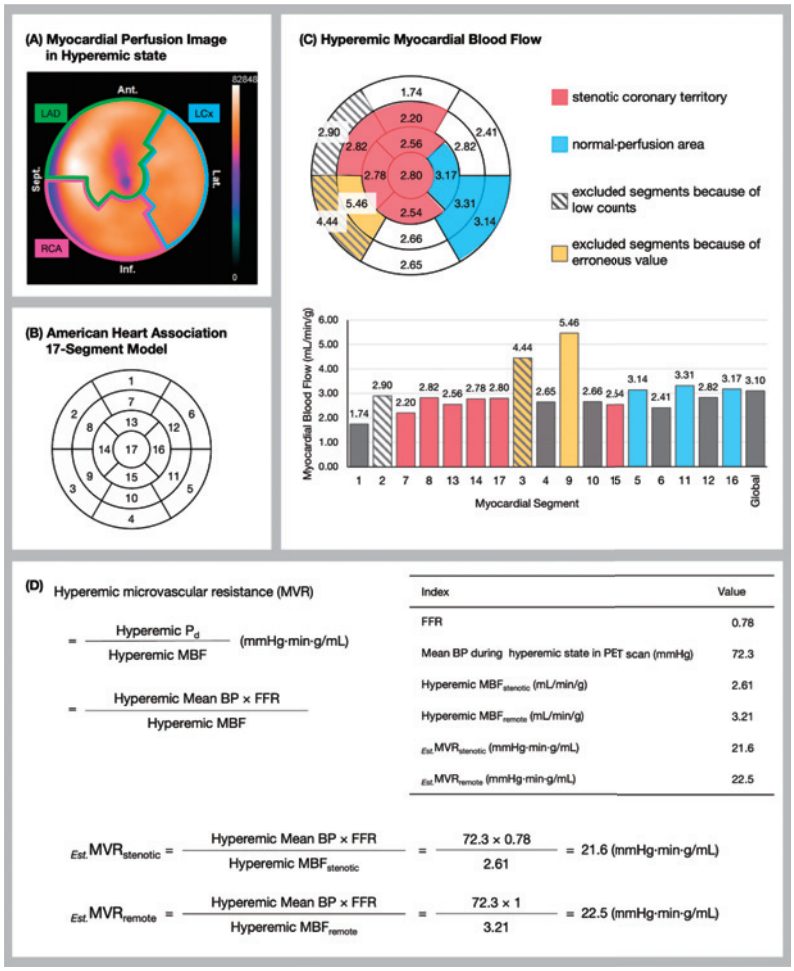

Fig. 1 Definition of the target territory and normal reference area and calculation of microvascular resistance (MVR)

(A) Polar map of myocardial perfusion image (MPI) in the hyperemic state, (B) the American Heart Association 17-segment model, and (C) the quantification value of hyperemic absolute myocardial blood flow (MBF). The major coronary artery territories are shown with standard myocardial model segmentation (A), and the left ascending coronary artery territory is shown with a green line. The red segments in (C) were the stenotic coronary territory adjusted by referring to MPI and coronary angiography. Thus, the mean hyperemic MBF in the stenotic coronary territory ($MBF_{stenotic}$) was 2.61 mL/min/g. The normal-perfusion area was defined as the 3 segments with the highest hyperemic MBFs, which were segments #5, 11, and 16 in this case (blue area in (C)), and the mean hyperemic MBF of these normal-perfusion area (MBF_{remote}) was 3.21 mL/min/g.

Formula (D) shows how MVR was calculated from the fractional flow reserve, absolute MBF, and mean blood pressure. The hyperemic MVR in the normal-perfusion area ($_{Est.}MVR_{remote}$) calculations assumed that FFR = 1. The hyperemic MVR in the stenotic coronary territory ($_{Est.}MVR_{stenotic}$) and $_{Est.}MVR_{remote}$ were 21.6 and 22.5 mm Hg·min·g/mL, respectively, with this formula.

Myocardial segments #2 and 3 (the gray diagonal stripes in (C)) and myocardial segments #3 and #9 (the yellow area in (C)) were not used to calculate hyperemic MBF_{remote}.

P_d, distal pressure; BP, blood pressure; $MBF_{stenotic}$, MBF in stenotic coronary territory; MBF_{remote}, MBF in normal-perfusion area; $_{Est.}MVR_{stenotic}$, hyperemic MVR in stenotic coronary territory; $_{Est.}MVR_{remote}$, hyperemic MVR in normal-perfusion area

ables as means and SDs, or medians and interquartile ranges, according to their distribution. Categorical variables were presented as count (%). The correlation between the absolute hyperemic MBF and MVR was assessed by using Pearson correlation coefficients (Pearson's r). A P value <0.05 was considered statistically significant. All statistical analyses were performed using SPSS version 19 (IBM Corp., Armonk, NY, USA).

Results

Among 69 vessels in 23 patients, visually significant stenosis was observed in an average of 4.8 (range, 3-8) myocardial segments, and FFR measurement was performed for 30 vessels (left ascending coronary artery, 22; left circumflex coronary artery, 6; and right coronary artery, 2). **Table 2** shows the breakdown of angiographic and FFR measurement results. A total of 22 vessels had visually significant stenosis (>50% stenosis) by CAG, and an FFR ≤0.75 was recorded in 13 vessels. **Table 3** shows the quantitative results for MBF, CFR, FFR, and MVR. The mean global MBF at rest and during hyperemia and mean global CFR were 1.02 ± 0.41 mL/min/g, 2.14 ± 1.05 mL/min/g, and 2.14 ± 1.08, respectively. The mean $_{Est.}MVR_{stenotic}$ and $_{Est.}MVR_{remote}$ were 33.2 ± 10.5 mm Hg・min・g/mL and 33.3 ± 8.0 mm Hg・min・g/mL. Twelve patients (52%) had a global CFR <2.0. The breakdown of the distribution of FFR and global CFR measurements is presented in **Figure 2**. The normal-perfusion area, which was composed of the 3 myocardial segments with the highest MBFs, most commonly included myocardial segment #8, followed by myocardial segments #9 and #11.

Table 2 Angiographic data

	All vessels (n = 30)	FFR ≤0.75 (n = 13)
LAD	22 (73%)	11 (50%)
RCA	6 (20%)	2 (33%)
LCx	2 (7%)	0 (0%)
Stenosis		
≤ 50%	8 (27%)	0 (0%)
51–75%	18 (60%)	11 (61%)
76% ≤	4 (13%)	2 (50%)

Data are presented as mean ± SD or number (%).
LAD, left anterior descending coronary artery; RCA, right coronary artery; LCx, left circumflex coronary artery

Relationship between $_{Est.}MVR_{stenotic}$ and $_{Est.}MVR_{remote}$ Hyperemic MBF_{remote} or CFR of the Normal Region

Figure 3A shows scatterplots illustrating the relationship between $_{Est.}MVR_{stenotic}$ and $_{Est.}MVR_{remote}$. **Figures 3B and 3C** shows scatterplots illustrating the relationship between the hyperemic MBF_{remote} or CFR of the normal region and $_{Est.}MVR_{stenotic}$. $_{Est.}MVR_{stenotic}$ and $_{Est.}MVR_{remote}$ were strongly positively correlated (r = 0.810, P < 0.01). Hyperemic MBF_{remote} and $_{Est.}MVR_{stenotic}$ were strongly negatively correlated (r = −0.758, P < 0.01), while the CFR of the normal region and $_{Est.}MVR_{stenotic}$ were moderately correlated (r = −0.587, P < 0.01). The equation below represents the estimated MVR calculated by the hyperemic MBF_{remote} and is based on the results of the correlation

Table 3 Quantitative analysis of PET and fractional flow reserve (FFR) measurements during invasive angiography

Acquisition data	Average	Median	Q1, Q3	Range
PET Perfusion Analysis				
Global rest MBF (mL/min/g)	1.02±0.41	1.02	0.87, 1.11	0.71—1.68
Global hyperemic MBF (mL/min/g)	2.14±1.05	2.07	1.75, 2.44	1.30—3.41
Global CFR	2.14±1.08	2.00	1.76, 2.57	1.36—3.31
Hyperemic MBF_{remote} (mL/min/g) (n=23)	2.55±1.08	2.47	2.18, 3.07	1.60—3.55
CFR of normal region (n=23)	2.71±1.40	2.63	2.11, 3.32	1.61—4.35
Hyperemic $MBF_{stenotic}$ (mL/min/g) (n=30)	2.04±1.21	1.84	1.68, 2.34	1.04—3.28
Invasive Coronary Angiography				
FFR (n=30)	0.80±0.22	0.78	0.72, 0.90	0.56—1.00
$_{Est.}MVR_{stenotic}$ (mm Hg·min·g/mL)	33.2±10.5	32.1	25.5, 41.0	15.1—59.1
$_{Est.}MVR_{remote}$ (mm Hg·min·g/mL)	33.3±8.0	31.7	27.9, 38.3	20.3—54.2
Mean blood pressure (mm Hg)	78.6±26.1	75.3	71, 85	60—108

Data are presented as mean ± SD or number (%).
Q1 indicates the first quartile; Q3, third quartile; MBF, myocardial blood flow; $MBF_{stenotic}$, MBF in stenotic coronary territory; MBF_{remote}, MBF in normal-perfusion area; CFR, coronary flow reserve; FFR, fractional flow reserve; MVR, microvascular resistance; $_{Est.}MVR_{stenotic}$, hyperemic MVR in stenotic coronary territory; $_{Est.}MVR_{remote}$, hyperemic MVR in normal-perfusion area.

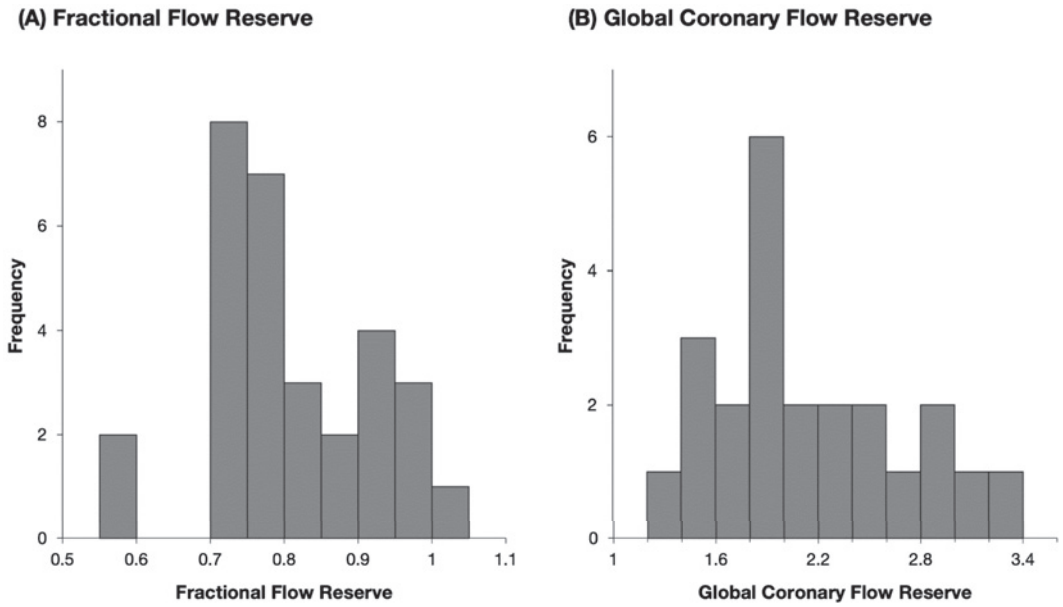

Fig. 2 Distribution of fractional flow reserve (FFR) and coronary flow reserve (CFR).
The distribution of FFR is presented as per-vessel analysis (A), and the distribution of the global CFR is presented as per-patient analysis (B).

scatterplots in **Figure 3B**.

$_{Est.}MVR_{stenotic} = 69.9 - 14.8 \times$ hyperemic MBF_{remote}.

Discussion

We found that $_{Est.}MVR_{stenotic}$ calculated from mean blood pressure, FFR and hyperemic $MBF_{stenotic}$ was strongly correlated with $_{Est.}MVR_{remote}$. Although $_{Est.}MVR_{stenotic}$ and $_{Est.}MVR_{remote}$ were MVRs calculated from MBF of different regions, they are nearly equivalent and $_{Est.}MVR_{stenotic}$ can be considered the MVR of the individual. These results suggest that deterioration of vasodilatory capacity is equivalent, with or without epicardial stenoses. In addition, $_{Est.}MVR_{stenotic}$ showed a strong correlation with hyperemic MBF_{remote}. These results suggest that hyperemic MBF_{remote} indicates CMD severity and can be used as an indicator of CMD severity. Thus, using quantitative MBF measurement with myocardial perfusion PET alone, physicians can detect early CMD, which could help prevent HFpEF or INOCA. However, the association between CFR in remote areas and $_{Est.}MVR_{stenotic}$ was weaker, perhaps because nonsignificant epicardial coronary atherosclerosis and some cardiac medications can affect rest MBF, which could weaken the correlation between CFR and $_{Est.}MVR_{stenotic}$.

The advantage of global CFR derived from perfusion PET is mainly in discriminating multivessel disease and estimating the risk of adverse cardiac events, in addition to traditional MPI with visual analysis, as has been reported in many studies[13–15]. Nevertheless, PET-MPI accounts for only a small percentage of all MPI procedures worldwide, and traditional visual analysis of MPI has been predominantly performed in routine clinical monitoring, even with PET. Most cardiologists and radiologists do not pay much attention to absolute myocardial blood flow values in clinical practice. Löffler et al. stated that global CFR is affected by epicardial flow-limiting stenosis and CMD, 2 major elements of ischemic heart disease, and they and Naya et al. state that it is difficult to evaluate these parameters separately in MPI[15,16]. Moreover, it appears that the normal range of MBF is difficult to determine. Sunderland et al. studied absolute MBF values in healthy individuals and reported that normal values for hyperemic MBF varied widely[8]. However, the present results suggest that variations in global hyperemic MBF might be explained simply as differences in coronary vasodilatation capability among individuals, which is easily estimated by MBF_{remote} areas, even in CAD patients. The concern that estimates of global CFR may be worse than is actually the case, because of reduced CFR in the stenotic area for coronary artery stenosis, is avoidable. Thus, the results of this and further studies may enhance the clinical usefulness of PET and improve understanding of the pathological mechanisms underlying chronic CAD. In addition, evaluation of atherosclerotic epicardial stenosis and CMD would deepen understanding of the pathological features of CAD and could modify standard decision-making regarding treatment strategy and risk stratification in patients with ischemic

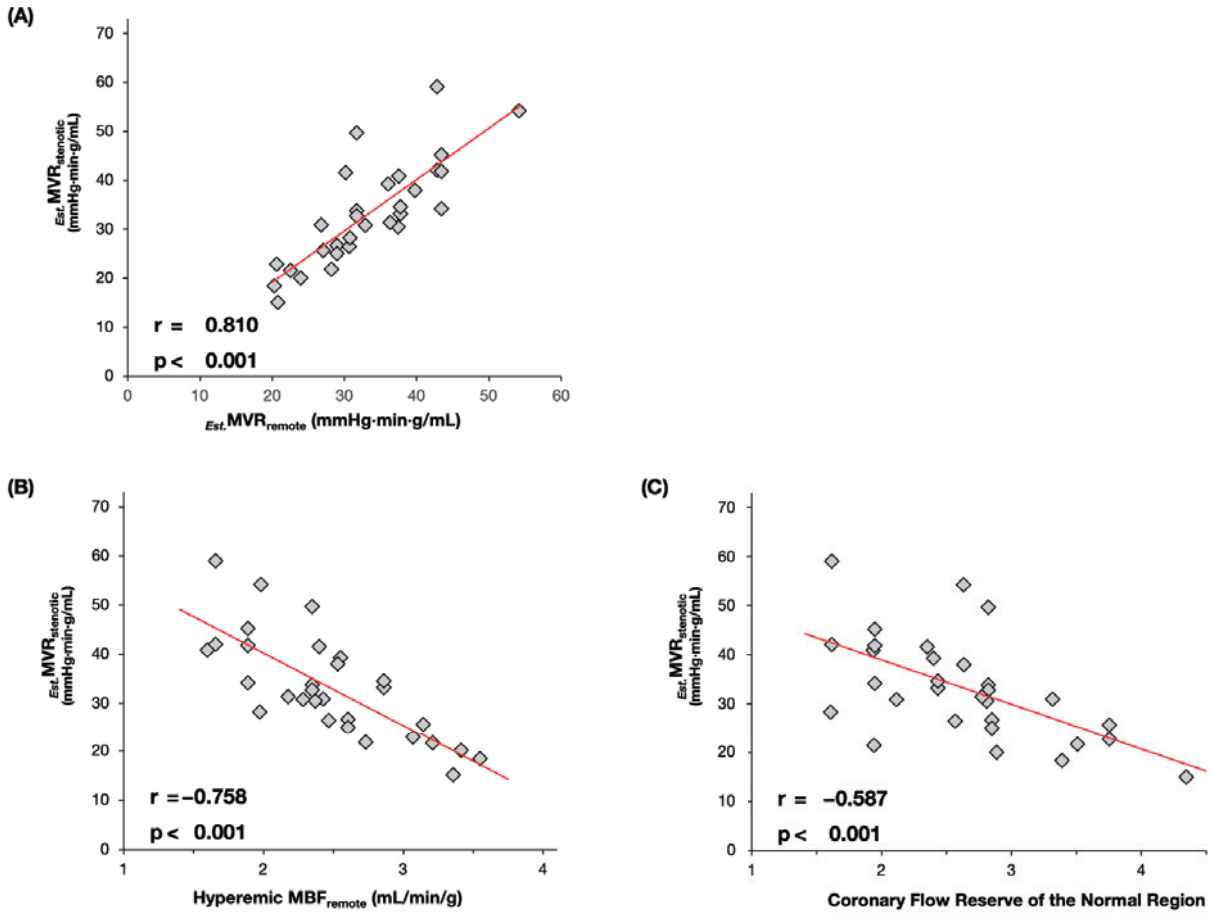

Fig. 3

Correlation between hyperemic microvascular resistance in stenotic coronary territory ($_{Est.}$MVR$_{stenotic}$) and hyperemic microvascular resistance in normal-perfusion area ($_{Est.}$MVR$_{remote}$) (A), the correlation between $_{Est.}$MVR$_{stenotic}$ and hyperemic myocardial blood flow of the normal-perfusion area (MBF$_{remote}$) (B), and the correlation between $_{Est.}$MVR$_{stenotic}$ and coronary flow reserve (CFR) of the normal-perfusion area (C). A strong positive correlation was observed between $_{Est.}$MVR$_{stenotic}$ and $_{Est.}$MVR$_{remote}$ (r = 0.810, P<0.01), as shown in (A). There was a strong negative correlation between $_{Est.}$MVR$_{stenotic}$ and hyperemic MBF$_{remote}$ (r = –0.758, P<0.01), but only a moderate correlation between $_{Est.}$MVR$_{stenotic}$ and CFR in the normal area (r = –0.587, P<0.01), as shown in (B) and (C). The estimated linear regression is shown as a straight red line in (B); $_{Est.}$MVR$_{stenotic}$ = 69.9 – 14.8 × hyperemic MBF$_{remote}$.

heart disease.

Recently, the ISCHEMIA trial illustrated the limitations of PCI for patients with chronic coronary disease[10]. This suggests that addressing imbalances in myocardial perfusion resulting from epicardial coronary stenosis with healed hard plaques was less meaningful than previously thought. Accordingly, detection of myocardial ischemia by MPI as an indicator of the need for elective PCI will be less relevant in the near future. This may have been largely influenced by the development of medical therapy, such as the use of strong statins, to prevent plaque formation, which reduces the morbidity and prevalence of acute coronary syndrome. In fact, the morbidity of acute coronary syndrome has decreased in developed countries worldwide. Therefore, evaluation of the severity of microvascular dysfunction, as well as assessment of imbalances in myocardial perfusion caused by atherosclerotic stenosis, should be a focus; however, in daily clinical practice much more attention should be paid to the prevalence of heart failure that is possibly related to microvascular dysfunction.

There are some inherent limitations in this study. First, it was conducted retrospectively at a single center. Second, MBF$_{stenotic}$, which was used to calculate $_{Est.}$MVR$_{stenotic}$, was overestimated because the definition of the stenotic coronary territory in this study was not identical to the actual stenotic coronary territory. Additionally, MVR estimated from PET acquisition data was not compared to MVR calculated by other modalities. Nevertheless, we believe that the estimated MVR in this study was meaningful because coronary microvascular function can be directly compared between patients. In the future, use of

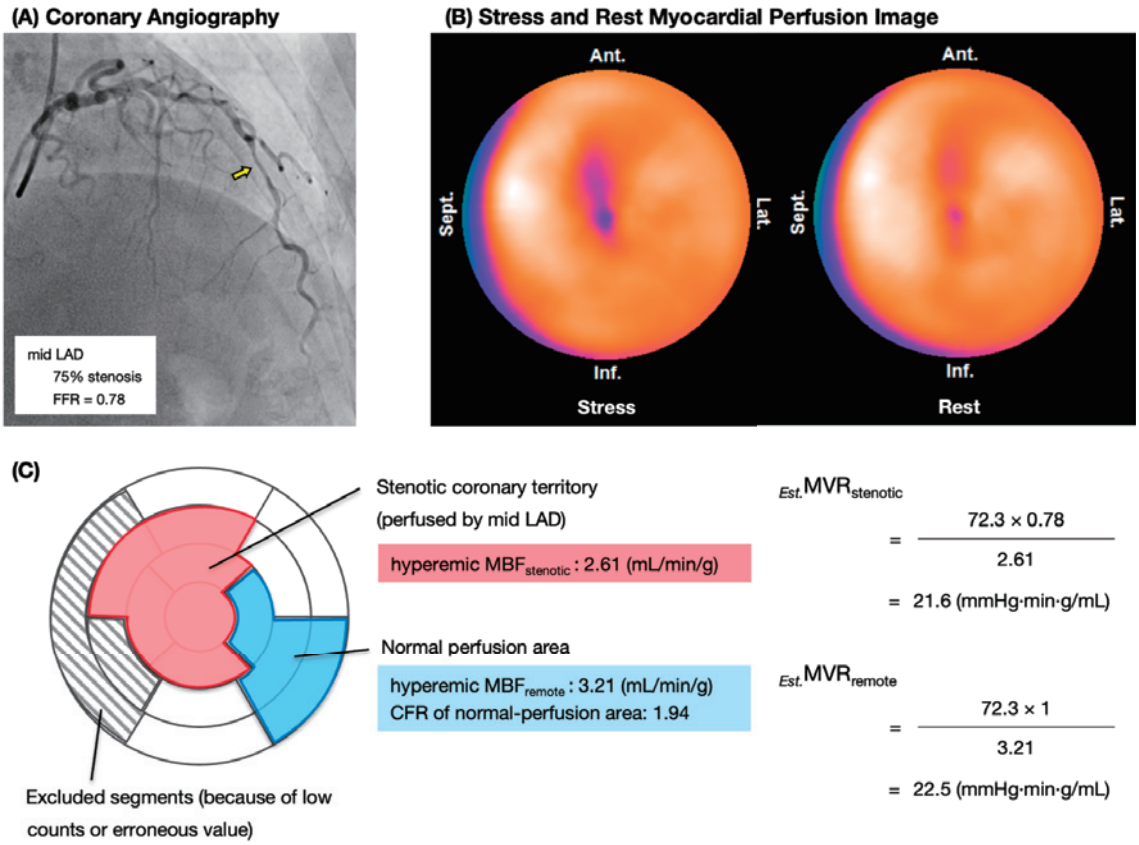

Fig. 4 Case

High hyperemic myocardial blood flow (MBF) and low microvascular resistance (MVR) were observed in a case of mid left anterior descending coronary artery stenosis in a 74-year-old woman with dyspnea on exertion. Invasive angiography was performed because of recent abnormal findings on an exercise stress electrocardiogram and coronary CT angiography. (A) Invasive coronary angiography demonstrated significant stenosis in the mid left anterior descending coronary artery (#7), and fractional flow reserve of the stenosis was 0.78. (B) Myocardial perfusion PET in hyperemia and the rest state showed ischemia of the mid-anteroseptal, apical, and distal inferior walls, which were considered to be perfused by the stenotic mid-left anterior descending coronary artery. The stenotic coronary territory is contoured as the red area in (C) by referring to angiography and perfusion PET image, which explains why the distal inferior wall was included the stenotic coronary territory. The normal-perfusion area was set in the 3 highest MBF segments as the blue area in (C). Mean blood pressure was 72.3 mm Hg in the hyperemic state PET scan. The hyperemic microvascular resistance in stenotic coronary territory was calculated as 21.6 mm Hg·min·g/mL.

a Voronoi diagram based on CT angiography will probably improve the accuracy of myocardial segmentation[17,18]. Third, the graph in **Figure 3B** shows the $_{Est.}MVR_{stenotic}$ estimating equation as a linear function; however, the relationship between resistance and flow should theoretically be inversely proportional. Because of the small sample size, our study may have predicted MVR using the linear equation. Finally, because this study included patients with multivessel disease, the area set as the remote may have included regions perfused by the stenotic epicardial arteries and may not be a true remote. However, mild stenosis does not reduce blood flow, and since pre-arterioles, arterioles, and capillaries are mainly involved in coronary resistance, stenosis of epicardial arteries has little effect on coronary resistance[19]. Despite these limitations, our findings are useful for diagnosis and development of treatment strategies.

Conclusions

The $_{Est.}MVR_{stenotic}$ was strongly associated with $_{Est.}MVR_{remote}$ and with hyperemic MBF_{remote} in ^{13}N-ammonia PET-MPI. The severity of microvascular disease in CAD patients with and without coronary artery stenosis might be estimated by determining the hyperemic MBF_{remote} of the normal-perfusion area with PET scans.

Conflict of Interest: None declared.

References

1. Camici PG, d'Amati G, Rimoldi O. Coronary microvascular dysfunction: mechanisms and functional assessment. Nat Rev Cardiol. 2015;12(1):48−62.
2. Camici PG, Crea F. Coronary microvascular dysfunction. N Engl J Med. 2007;356(8):830−40.
3. Berry C, Corcoran D, Hennigan B, Watkins S, Layland J, Oldroyd KG. Fractional flow reserve-guided management in stable coronary disease and acute myocardial infarction: recent developments. Eur Heart J. 2015;36(45):3155−64.
4. Marinescu MA, Löffler AI, Ouellette M, Smith L, Kramer CM, Bourque JM. Coronary microvascular dysfunction, microvascular angina, and treatment strategies. JACC Cardiovasc Imaging. 2015;8(2):210−20.
5. Taqueti VR, Di Carli MF. Coronary Microvascular Disease Pathogenic Mechanisms and Therapeutic Options: JACC State-of-the-Art Review. J Am Coll Cardiol. 2018;72(21):2625−41.
6. Brainin P, Frestad D, Prescott E. The prognostic value of coronary endothelial and microvascular dysfunction in subjects with normal or non-obstructive coronary artery disease: A systematic review and meta-analysis. Int J Cardiol. 2018;254:1−9.
7. Fearon WF, Kobayashi Y. Invasive Assessment of the Coronary Microvasculature: The Index of Microcirculatory Resistance. Circ Cardiovasc Interv. 2017;10(12):e005361.
8. Sunderland JJ, Pan XB, Declerck J, Menda Y. Dependency of cardiac rubidium-82 imaging quantitative measures on age, gender, vascular territory, and software in a cardiovascular normal population. J Nucl Cardiol. 2015;22(1):72−84.
9. Boden WE, O'Rourke RA, Teo KK, et al. Optimal medical therapy with or without PCI for stable coronary disease. N Engl J Med. 2007;356(15):1503−16.
10. Maron DJ, Hochman JS, Reynolds HR, et al. Initial Invasive or Conservative Strategy for Stable Coronary Disease. N Engl J Med. 2020;382(15):1395−407.
11. DeGrado TR, Hanson MW, Turkington TG, et al. Estimation of myocardial blood flow for longitudinal studies with 13N-labeled ammonia and positron emission tomography. J Nucl Cardiol. 1996;3(6 Pt 1):494−507.
12. Lee JM, Hwang D, Park J, et al. Exploring Coronary Circulatory Response to Stenosis and Its Association With Invasive Physiologic Indexes Using Absolute Myocardial Blood Flow and Coronary Pressure. Circulation. 2017;136(19):1798−808.
13. Sciagrà R, Lubberink M, Hyafil F, et al. EANM procedural guidelines for PET/CT quantitative myocardial perfusion imaging. Eur J Nucl Med Mol Imaging. 2021;48(4):1040−69.
14. Taqueti VR, Hachamovitch R, Murthy VL, et al. Global coronary flow reserve is associated with adverse cardiovascular events independently of luminal angiographic severity and modifies the effect of early revascularization. Circulation. 2015;131(1):19−27.
15. Naya M, Murthy VL, Taqueti VR, et al. Preserved coronary flow reserve effectively excludes high-risk coronary artery disease on angiography. J Nucl Med. 2014;55(2):248−55.
16. Löffler AI, Bourque JM. Coronary Microvascular Dysfunction, Microvascular Angina, and Management. Curr Cardiol Rep. 2016;18(1):1.
17. Kurata A, Kono A, Sakamoto T, et al. Quantification of the myocardial area at risk using coronary CT angiography and Voronoi algorithm-based myocardial segmentation. Eur Radiol. 2015;25(1):49−57.
18. Fukuyama N, Kido T, Kurata A, et al. Myocardial Segmentation of Area at Risk Based on Coronary Computed Tomography Angiography and Voronoi Diagram in Comparison with Magnetic Resonance Perfusion Imaging. Open J Radiol. 2017;7:9−22.
19. Del Buono MG, Montone RA, Camilli M, et al. Coronary Microvascular Dysfunction Across the Spectrum of Cardiovascular Diseases: JACC State-of-the-Art Review. J Am Coll Cardiol. 2021;78(13):1352−71.

(Received, October 26, 2022)

(Accepted, December 28, 2022)

(J-STAGE Advance Publication, February 21, 2023)